

## Electronic Supporting Information (ESI)

### Homospin Single-chain magnet with 1D ferromagnetic azido-cobalt Ising-type chain

Zuo-Xi Li, Yong-Fei Zeng, Hong Ma, and Xian-He Bu\*

*Department of Chemistry, and TKL of Metal- and Molecule-Based Material Chemistry, Nankai University, Tianjin 300071, China. Fax: 86 22 2350-2458; E-mail: buxh@nankai.edu.cn*

#### Single-crystal X-ray diffraction

X-ray single-crystal diffraction data was collected on a Rigaku R-axis rapid IP area detector with graphite monochromatic Mo-K $\alpha$  radiation ( $\lambda = 0.71073 \text{ \AA}$ ). The program SAINT<sup>1</sup> was used for integration of the diffraction profiles. The crystal structure was solved by direct methods using the SHELXS program of the SHELXTL package and refined by full-matrix least-squares methods with SHELXL<sup>2</sup>. Metal atoms were located from the *E*-maps and other non-hydrogen atoms were located in successive difference Fourier syntheses and refined with anisotropic thermal parameters on *F*<sup>2</sup>. Hydrogen atoms were generated theoretically onto the specific atoms and refined isotropically with fixed thermal factors.

#### References

- (1) Bruker AXS, *SAINT Software Reference Manual*, Madison, WI, **1998**.
- (2) Sheldrick, G. M. *SHELXTL NT Version 5.1. Program for Solution and Refinement of Crystal Structures*, University of Göttingen, Germany, **1997**.

#### General experimental procedures

Elemental analyses of C, H and N were performed on a Perkin-Elmer 240C analyzer. IR spectra were measured on a TENSOR 27 (Bruker) FT-IR spectrometer with KBr pellets. The X-ray powder diffraction (XRPD) was recorded on a Rigaku D/Max-2500 diffractometer at 40 kV, 100 mA for a Cu-target tube and a graphite monochromator. Magnetic data were collected on a Quantum Design MPMS-XL7 superconducting quantum interference device (SQUID) magnetometer equipped with a 5T magnet using crushed crystals of the sample at Nankai University. The diamagnetic corrections were calculated using Pascal's constants. The samples were grinded and fixed by eicosane to avoid movement during the measurement.

**Table S1.** Selected bond lengths [ $\text{\AA}$ ] and angles [ $^\circ$ ] for **1**.

---

Co(1)-N(4)#1	2.101(5)	Co(1)-N(4)	2.101(5)
Co(1)-N(1)#2	2.239(6)	Co(1)-N(1)#3	2.239(6)
Co(1)-N(1)#1	2.244(6)	Co(1)-N(1)	2.244(6)
N(4)#1-Co(1)-N(1)#2	89.4(2)	N(1)#2-Co(1)-N(1)	76.4(2)
N(4)-Co(1)-N(1)#2	90.6(2)	N(4)#1-Co(1)-N(1)#3	90.6(2)
N(4)-Co(1)-N(1)#3	89.4(2)	N(1)#3-Co(1)-N(1)	103.6(2)
N(4)#1-Co(1)-N(1)#1	90.1(2)	N(4)-Co(1)-N(1)#1	89.9(2)
N(1)#2-Co(1)-N(1)#1	103.6(2)	N(1)#3-Co(1)-N(1)#1	76.4(2)
N(4)#1-Co(1)-N(1)	89.9(2)	N(4)-Co(1)-N(1)	90.1(2)
Co(1)#4-N(1)-Co(1)	103.6(2)		

\*Symmetry mode, #1 -x+2, -y+1, -z+1; #2 -x+1, -y+1, -z+1; #3 x+1, y, z; #4 x-1, y, z.

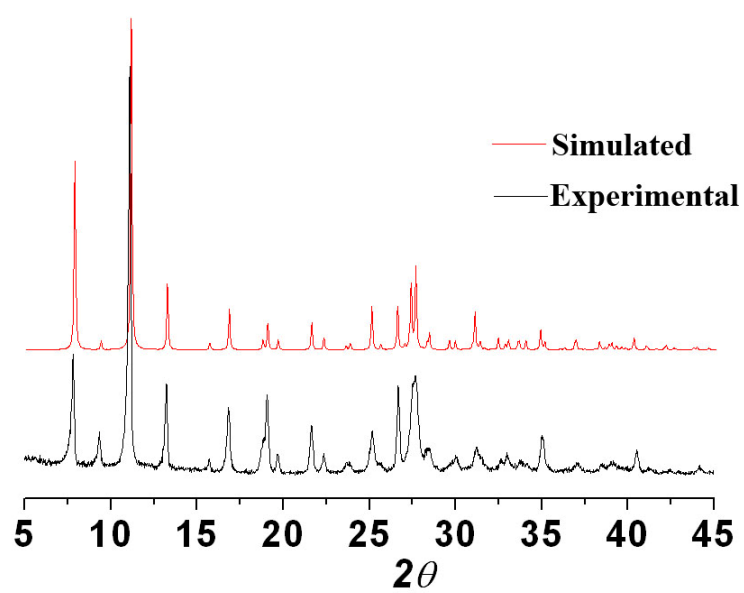


**Fig. S1** The simulated and experimental powder XRD patterns for **1**.

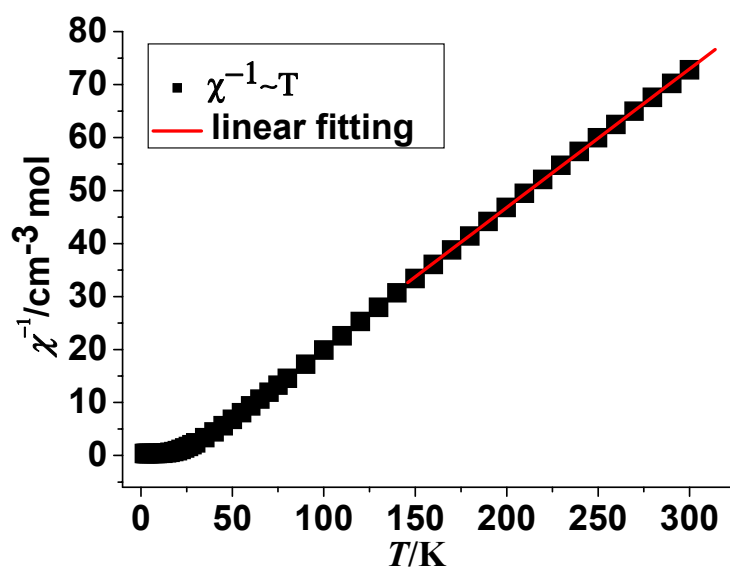


Fig. S2  $\chi^{-1}$  vs  $T$  plot and the solid line is the best fit to Curie-Weiss law.

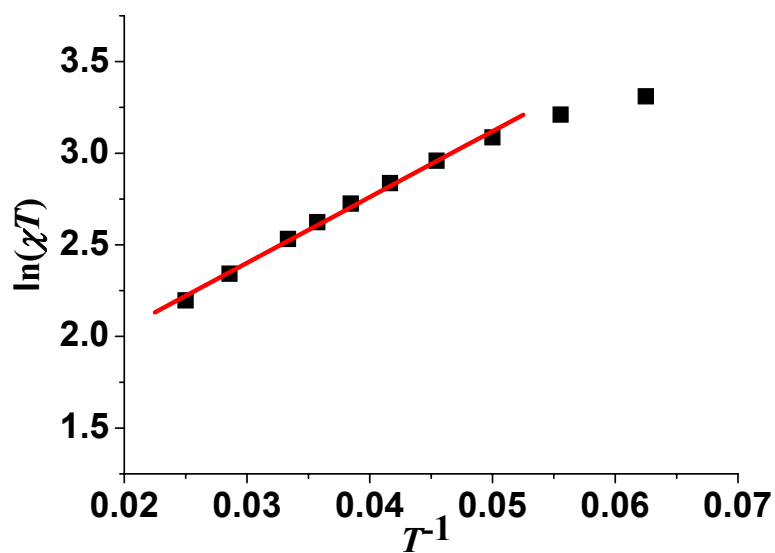
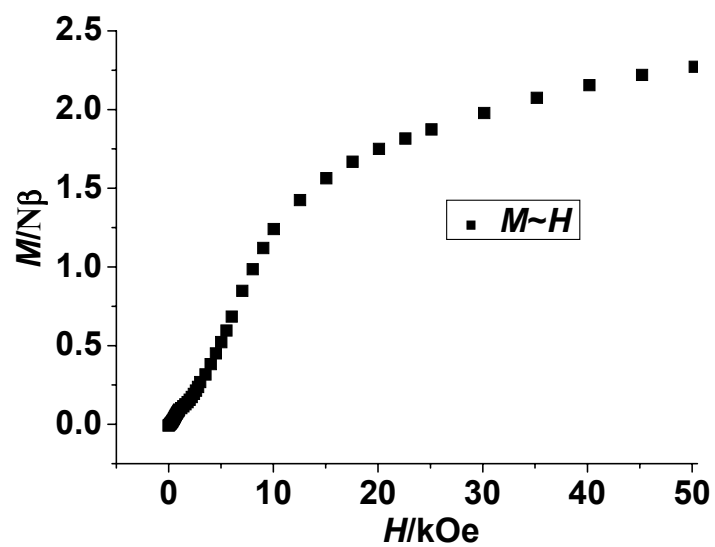


Fig. S3 The plot of  $\ln(\chi T)$  vs  $1/T$  at low temperature range and its fitting line



**Fig. S4** Field-dependent isothermal magnetization curve at 2 K